Volume 16 | Number 8 | 28 February 2014 | Pages 1397–1594

CrystEngComm

www.rsc.org/crystengcomm

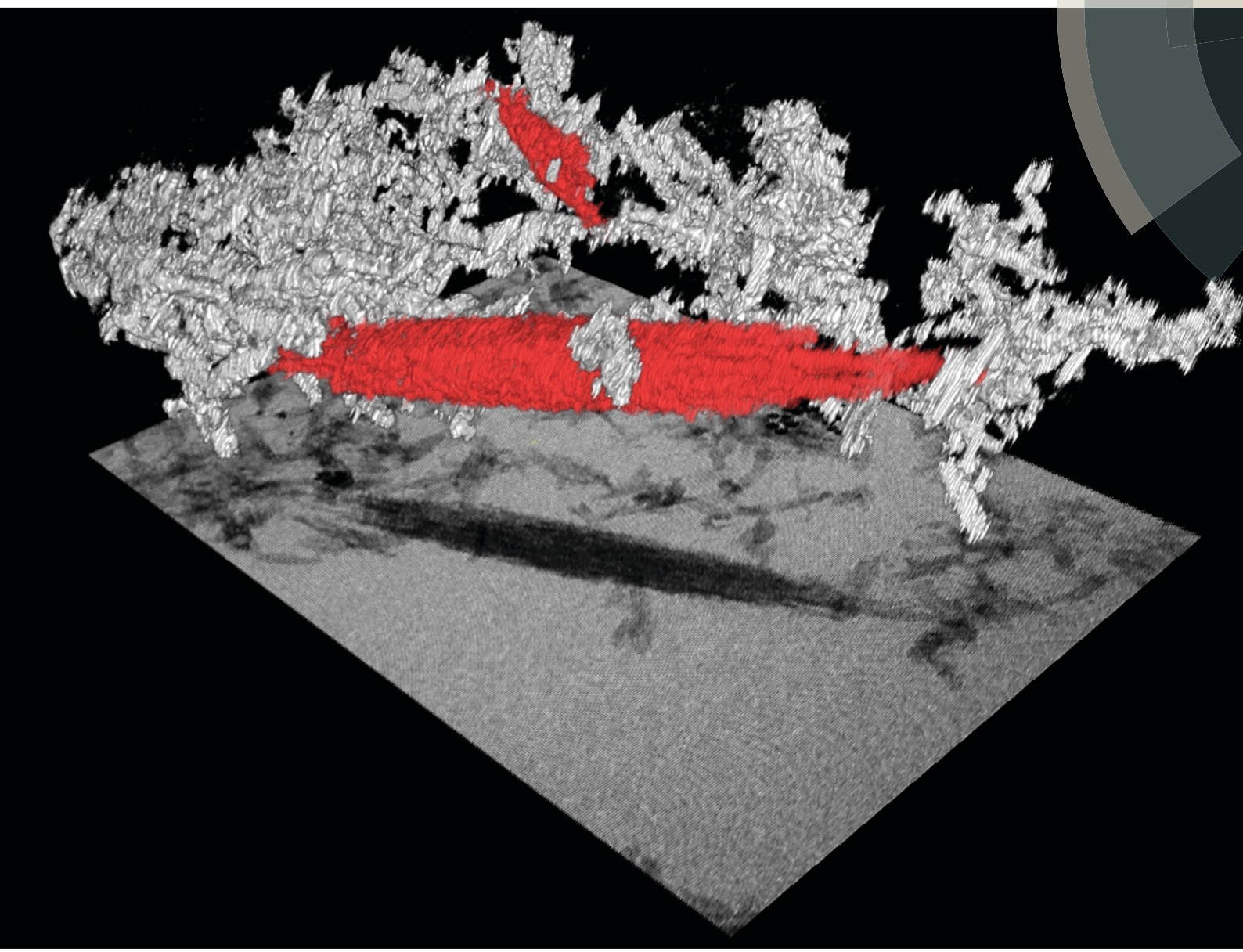

ROYAL SOCIETY OF CHEMISTRY

COVER ARTICLE

Frandsen, Banfield *et al.*

Aggregation-induced growth and transformation of β-FeOOH nanorods to micron-sized α-Fe_2O_3 spindles

CrystEngComm

PAPER

View Article Online
View Journal | View Issue

Cite this: *CrystEngComm*, 2014, **16**, 1451

Aggregation-induced growth and transformation of β-FeOOH nanorods to micron-sized α-Fe_2O_3 spindles

Cathrine Frandsen,†*[ab] Benjamin A. Legg,†[a] Luis R. Comolli,[c] Hengzhong Zhang,[a] Benjamin Gilbert,[d] Erik Johnson[e] and Jillian F. Banfield*[a]

Received 31st May 2013,
Accepted 21st October 2013

DOI: 10.1039/c3ce40983j

www.rsc.org/crystengcomm

Intimate interconnection of crystal growth, (oriented) aggregation and phase transformation seem common in the formation of nano- and microcrystalline materials from solutions. Yet, the mechanistic linkages between the different processes have not been fully understood. In this work, we studied the hydrothermal growth of akaganeite (β-FeOOH) nanorods and their transformation to micron-sized hematite (α-Fe_2O_3) spindles using high-resolution cryogenic transmission electron microscopy (cryo-TEM). Only akaganeite particles and hematite spindles were detected in the samples. Further, cryo-electron 3D tomograms show that akaganeite nanorods were aggregated into loose three-dimensional networks with some embedded hematite spindles. Based on our cryo-TEM and additional X-ray diffraction, electron microscopy, and chemical data, we propose the following mechanism: first, formation of the early-stage hematite spindles is driven by phase stability change due to increase in size caused by oriented aggregation of akaganeite. Then, akaganeite particles continue to transform to hematite upon contact with and recrystallization onto hematite surfaces, making hematite grow with a constant aspect ratio and forming micron-sized nano-porous single-crystal spindles. Our growth model interprets experimental observations well and it resolves previous long-time debate over whether the hematite spindles are formed *via* classical Ostwald ripening or by oriented aggregation of hematite nanoparticles. Possibly, this aggregation-based concurrent growth and transformation model may also be applicable to crystal growth and phase transformation in other systems.

Introduction

In nanomaterials, aggregation, crystal growth, and phase stability can be interconnected. For example, 5 nm amorphous silica spheres may aggregate into 30–50 nm diameter particles that transform to single silicate crystals while retaining the size and shape of the precursor aggregate.[1] Another example is ferrihydrite particles, a few nm in diameter, that form loose rod-shaped aggregates which later fuse into straight, single-crystalline goethite (α-FeOOH) rods.[2] Moreover, a study has reported how secondary crystals of magnetite (Fe_3O_4) can continue to grow by addition and transformation of amorphous precursor particles.[3] The apparently tight mechanistic linkages between particle aggregation and phase transition seem relevant for describing (non-classical) crystal growth processes.

Iron (oxyhydr)oxides provide an interesting system for the development of models to explain linkages among aggregation, phase transformation and morphology development, because environmentally driven phase transitions and aggregation-based growth of iron (oxyhydr)oxides have been widely reported.[4–6] Additionally, iron (oxyhydr)oxide systems are important in many natural settings and industrial applications, and understanding the interplay between growth, nanocrystallinity, and phase transitions is important for understanding and controlling *e.g.*, availability of (heavy) ions in water systems, corrosion processes, pigment productions, magnetic data bit formation, and metallurgy.

The formation of micron-sized α-Fe_2O_3 (hematite) particles from β-FeOOH (akaganeite) precursor nanoparticles has been reported under hydrothermal conditions.[7,8] The final product is monodisperse single hematite crystals. There has been

[a] *Department of Earth and Planetary Science, University of California, Berkeley, CA 94720, USA. E-mail: jbanfield@berkeley.edu*
[b] *Department of Physics, Technical University of Denmark, 2800 Kgs. Lyngby, Denmark. E-mail: fraca@fysik.dtu.dk*
[c] *Life Sciences Division, Lawrence Berkeley National Laboratory, Berkeley, CA 94720, USA*
[d] *Earth Sciences Division, Lawrence Berkeley National Laboratory, Berkeley, CA 94720, USA*
[e] *Niels Bohr Institute, University of Copenhagen, 2100 Copenhagen, Denmark*
† These authors contributed equally.

considerable debate as to whether the hematite particles form by aggregation of hematite nanoparticles[9–11] or instead by dissolution and reprecipitation.[8,12]

Here, we analyzed the growth of akaganeite and its transformation to hematite in aqueous solution using a combination of hydrothermal experiments, high-resolution transmission electron microscopy (HRTEM), cryogenic transmission electron microscopy (cryo-TEM), chemical analysis, and synchrotron X-ray diffraction. We propose a new growth model in which aggregation of primary akaganeite particles and also aggregation of akaganeite particles onto hematite precede phase transformation.

Experiments

Nanoparticle suspensions were prepared from an aqueous solution containing 20 mM $FeCl_3$ and 0.45 mM NaH_2PO_4. Solutions were filtered through 0.2 μm pores and placed in closed Pyrex bottles. Precipitation was induced by heating in a preheated oven at 100 °C for up to 7 days, following the method of ref. 7 and 10. Phosphate was added to the synthesis to induce formation of spindle-shaped hematite that is partly transparent to TEM. Without phosphate, micron-sized pseudo-cubes of hematite form.[9] It has been suggested that phosphate ions adsorb more strongly to the (*hk*0) crystal faces of hematite, and hence growth along the *c*-axis is favored.[13] In our experiments, the particle growth and transformation processes were documented by removing a series of bottles from the oven at different time points. Containers were cooled by immersion in cold running water. The samples were stored in solution at room temperature prior to analysis.

Synchrotron X-ray diffraction patterns of dried suspensions were measured at the Advanced Light Source, Lawrence Berkeley National Laboratory, beam line 11-3-1 (photon wavelength λ = 0.729294 Å).

Transmission electron microscopy (TEM) images of particle suspensions after 23, 56, 71, 102 and 166 h of heat treatment, drop-casted and dried onto holey amorphous carbon films, were obtained using a JEOL 200CX microscope and a FEI Technai microscope at the National Centre for Electron Microscopy, Lawrence Berkeley National Laboratory.

2D and 3D cryo-TEM images were acquired using a JEOL-3100-FFC electron microscope equipped with a FEG electron source operating at 300 kV, an Omega energy filter (JEOL), cryo-transfer stage, and a Gatan 795 2K × 2K CCD camera (Gatan Inc., Pleasanton, CA, USA) at the Life Science Division, Lawrence Berkeley National Laboratory. Prior to sample addition, carbon-coated Lacey Formvar support grids (Ted Pella) were pretreated by plasma discharge to induce sample wetting. Citrate-capped, 10 nm colloidal gold particles (BB International) were added to the grid to serve as fiducial markers for image alignment. A ~4 μL drop of sample suspension was added to each grid. Excess solution was removed by blotting with cellulose filter paper, leaving a thin film, between 100 and 400 nm thick, which is immediately plunged into liquid ethane at −180 °C. This transforms the solution to vitreous ice, allowing particles and aggregate structures to be imaged directly in the TEM.

Five tomographic datasets, at magnifications of 50k× to 110k×, were produced by acquiring a tilt series, over a range of ±65 degrees, at 2° increments. Image alignment was achieved by fiducial tracking with etomo.[14] Fiducial particles were digitally removed and a 3D reconstruction was computed using tomo3d.[15] The tomogram was converted into a 3D binary image, using the automated trainable segmentation algorithm in FIJI.[16]

Size selective ultra-centrifugation (up to 300k rcf for 30 minutes) was used to sediment out increasingly smaller particles, allowing us to isolate very large and very small particles for further analysis by X-ray diffraction, *via* PANalytical X'Pert Pro diffractometer with a Co source (Kα λ = 1.79021 Å). After the final centrifugation step, the dissolved iron concentrations in the remaining supernatant solutions (which are colorless and transparent) were measured using UV–Vis spectroscopy with ferron dye (600 nm adsorption band).[17] This chemical assay is only sensitive to dissolved iron species.

Results

Upon heating aqueous solutions containing 20 mM $FeCl_3$ and 0.45 mM NaH_2PO_4 at 100 °C for <1 hour, samples changed from their original translucent yellow color to a translucent deep red-brown color. After heating for ~50 hours, the samples became cloudy, and after 60 hours of aging the color turns more orange-brown and particle sedimentation occurs. The pH of the ferric solutions drops from 2.2 before heat treatment to 1.5–1.6 afterwards.

Ferron assay measurements of the dissolved supernatant iron concentration in centrifuged samples showed a decrease from 20 mM to 10.0 mM after 1 hour and a continuous decrease with increasing heating time to a value of 0.9 mM after 167 hours.

Fig. 1a shows synchrotron X-ray diffraction data at aging times from 15 hours to 102 hours. At early times, all diffraction lines were from akaganeite, indicating that akaganeite is the dominant phase. Hematite remains below the detection limit until 56 h of aging. By 65 h, hematite is abundant. Only trace amounts of akaganeite can be detected by X-ray diffraction after 88 hours, indicating almost complete replacement (in wt%) of this phase by hematite.

Rietveld total pattern fitting was performed to determine the mass fraction of each phase and respective particle sizes over time using MAUD.[18] Akaganeite ($I2/m$) lattice parameters[19] (a, b, c, β) were refined by fitting the 15 h sample to a = 10.587 Å, b = 3.032 Å, c = 10.513 Å and β = 90.41°. Hematite ($R\bar{3}c$) lattice parameters[20] (a, c) were refined by fitting the data from the 102 h sample to a = 5.032 Å and c = 13.800 Å. The mass fraction of each phase was obtained from whole pattern analysis of intermediate time-point X-ray data, with particle size and abundances as free refinement parameters. Fits of all data are good (Rwp% always less than 10, but typically between 2.6 and 4.6). The mass fraction curve was fit

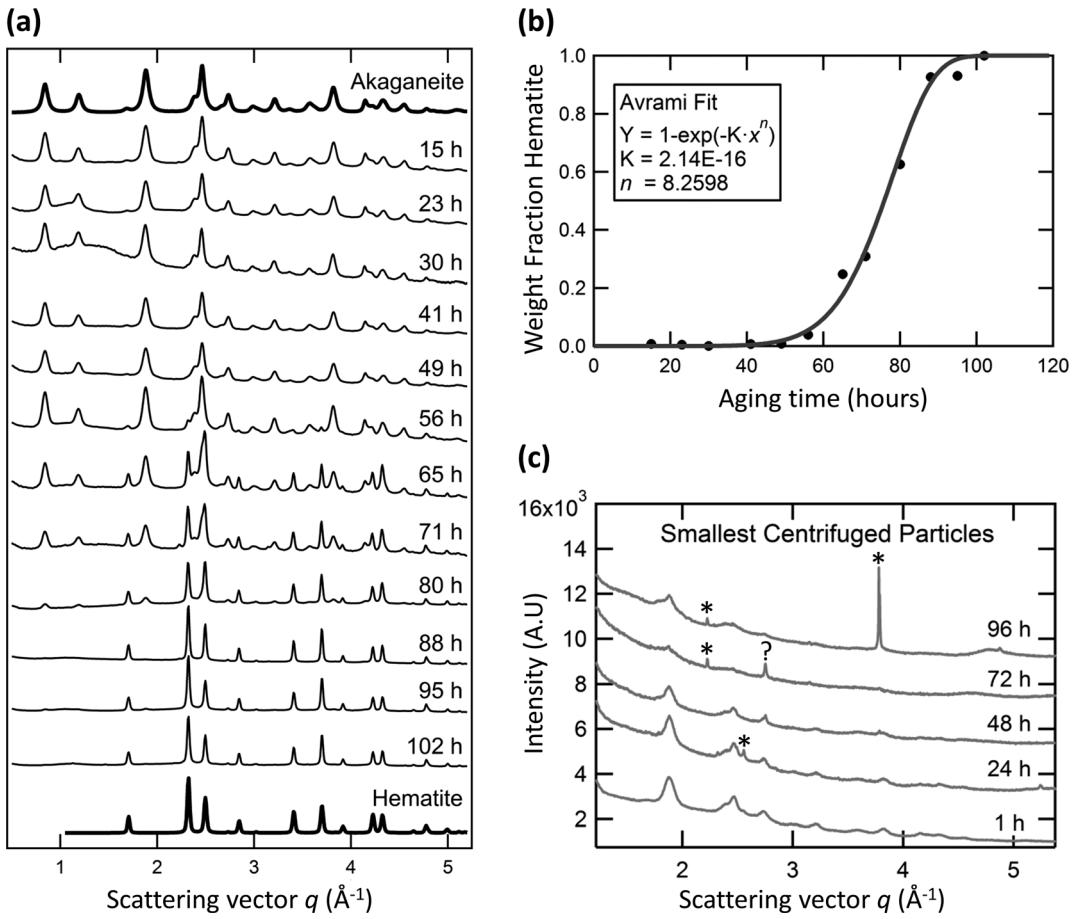

Fig. 1 X-ray diffraction. (a) Synchrotron X-ray data of samples heat treated for 15–102 h. The top and bottom curves show computed, refined curves for 100% akaganeite and 100% hematite, respectively. (b) Weight fraction hematite with treatment time, obtained from (a); solid curve represents Avrami fit to data. (c) X-ray diffraction (Co Kα λ) of the smallest particles in samples after heat treatment for 1–96 h. The narrow diffraction peaks in (c) denoted with asterisks are from the Si-substrate, the 2.82 *d*-spacing on 72 h data denoted ? is unidentified but not hematite.

using an Avrami transformation model (Fig. 1b). An Avrami exponent of 8.3 was obtained. An Avrami exponent of >4 suggests non-standard growth kinetics, with rapid transformation following a significant incubation period.[21]

TEM images of the samples taken after different times of heat treatment (examples shown in Fig. 2 and 3) showed, in particular, two particle types with different morphologies: rods of akaganeite and larger spindle-shaped hematite, as expected based on our synthesis approach.[7,10,12] Particle phases were identified from lattice fringe spacing. At early aging times, the akaganeite particles dominated but TEM also revealed that some spindle-shaped hematite particles were present after 23 h of treatment. In correspondence with TEM observations, X-ray diffraction of size selective samples obtained by centrifugation of samples aged for 1, 24, 48, 72, 96 h showed that the largest size particle fractions contain hematite if samples had been aged for 24 hours or more.

TEM images also revealed a subset of very small particles with pseudo-spherical shape and size ≤5 nm (circled in Fig. 2c). Although previous authors[11] posited the existence of small hematite particles, we found no evidence of them. X-ray diffraction patterns obtained for the smallest size fractions of samples aged for 1, 24, 48, 72, and 96 h only revealed akaganeite (Fig. 1c).

We used TEM images to measure the lengths and widths of akaganeite rods and hematite spindles in samples aged for 23, 49, 56, 71, 102, and 166 h. The lengths and widths of 300 akaganeite particles were measured in samples from each time point. The particle sizes of akaganeite were calculated as length times width squared, and the particle size distribution fit with a log-normal distribution (number weighted). Fig. 4a shows the evolution of the akaganeite particle size distribution, with the populations normalized to reflect the total amount of akaganeite in the suspension, as estimated from Rietveld refinement of synchrotron X-ray diffraction patterns. The mean particle size increased over time, with a very slight narrowing in the distribution breadth. This is due to an increase in mean particle width from 7.6 ± 2.3 nm to 11.5 ± 2.5 nm and decrease in the mean particle length over time. Particle aspect ratio decreases monotonically from a value of 3.3 ± 1.9 at 23 hours, to 1.7 ± 0.8 at 102 hours (Fig. 4b). Hematite particles grew with a constant aspect ratio of 6–7 and increased in length from 200 ± 30 nm at 23 h to 580 ± 30 nm at 71 h and 670 ± 60 nm at 166 h (Fig. 4c).

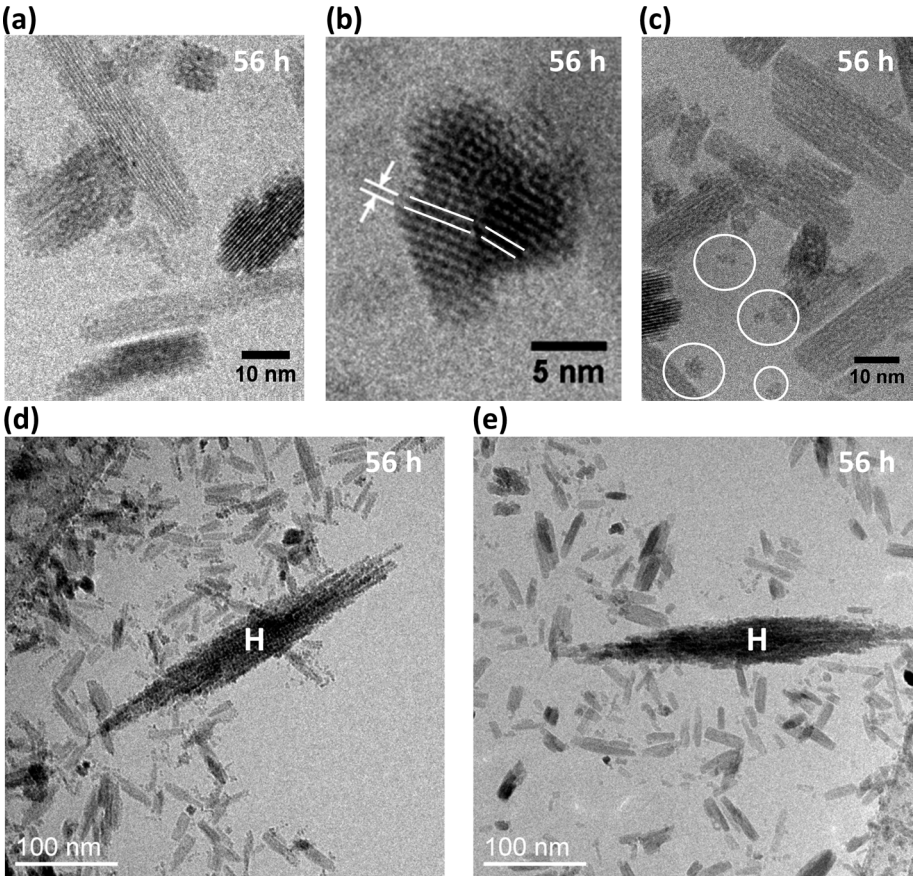

Fig. 2 Cryo-TEM images, after 56 h heat treatment. (a)–(c) High-resolution images of akaganeite rods. Lattice spacing in (b) is ~0.74 nm. White circles in (c) surround very small akaganeite particles. (d)–(e) Broad-field views showing connectivity of akaganeite particles and hematite spindles (H).

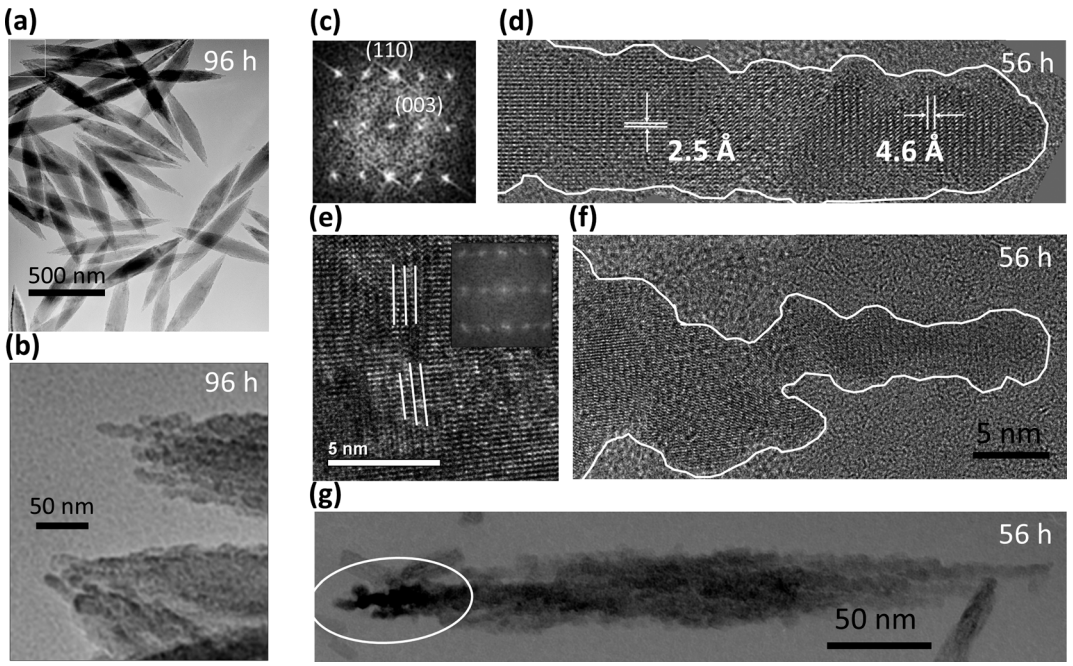

Fig. 3 TEM images of hematite spindles, after 56 h and 96 h. White-boxed area in (a) is enlarged in (b). Fast-Fourier transformed images in (c) and (e) show aligned and nearly aligned nanocrystalline grains in protruding spindle ends like those in (d) and (f). White ellipsoid in (g) surrounds contrast from hematite grains with different crystalline orientation.

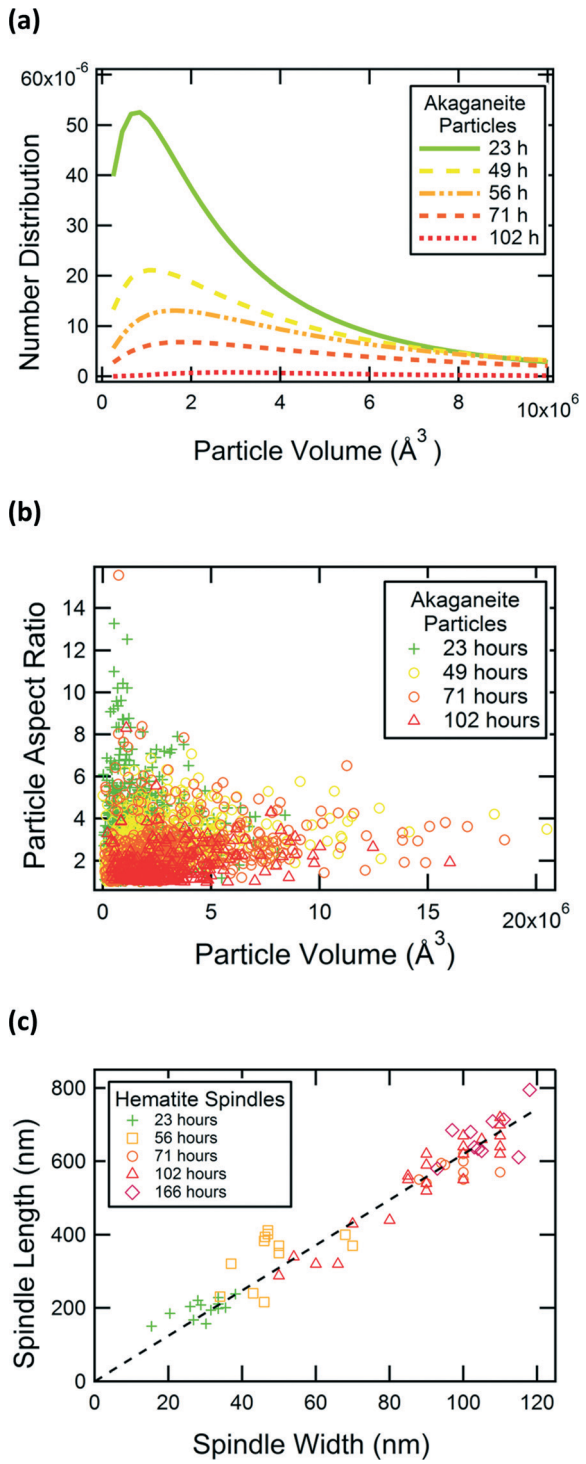

Fig. 4 Particle growth with heat treatment time. (a) Particle size distribution of akaganeite. (b) Aspect ratio of akaganeite particles. (c) Hematite spindles' width and length.

High-resolution TEM images showed akaganeite rods are elongated along their *b* axis. Cryo-TEM analyses achieved lattice fringe resolution for akaganeite nanoparticles in a sample recovered after 56 h of treatment. Preservation in vitrified ice allowed us to visualize the akaganeite rods in multiple orientations, including side- and end-on (Fig. 2a, b), and to capture particle arrangements as *in aqua*. As also seen in conventional TEM analysis (data not shown), small groups of akaganeite rods were often crystallographically aligned and primarily attached on their (100) and (001) surfaces. The small discrepancy in lattice parameters for the *a* and *c* axes in akaganeite's monoclinic structure can lead to low angle grain boundaries, as observed in Fig. 2b.

The hematite spindles are much larger than the akaganeite rods and are nano-porous. The hematite spindles typically diffract as single crystals, but their outlines are very irregular and they appear to be composed of several thousand crystallographically aligned subparticles (3–5 nm thick) (Fig. 3a, b). The hematite spindles and their nanoporous structure are elongated along the hexagonal *c* axis of hematite (Fig. 3c, d). Substructure is most apparent where component units protrude from the spindle ends. Irregularities on hematite crystal surfaces (Fig. 3b, d, f, g) have shapes similar to those of primary akaganeite nanoparticles. Occasionally, low-angle grain boundaries are present within the hematite spindles (Fig. 3e). In addition, we sometimes observed diffraction contrast between adjacent regions of hematite (see white circle in Fig. 3g), suggesting domains in slightly different crystallographic orientations.

Slices of TEM tomograms obtained for a hematite spindle after 56 h of aging revealed an irregular external surface and high internal porosity (see cross sections in Fig. 5a, b). With further aging time, the internal porosity appeared to decrease, but some porosity remained even after 96 h of aging (Fig. 3b).

TEM images of dried samples suggest that akaganeite and hematite particles are co-aggregated (Fig. 3g); however, these results may be influenced by drying artifacts. Cryo-TEM analysis circumvented this problem by directly imaging the

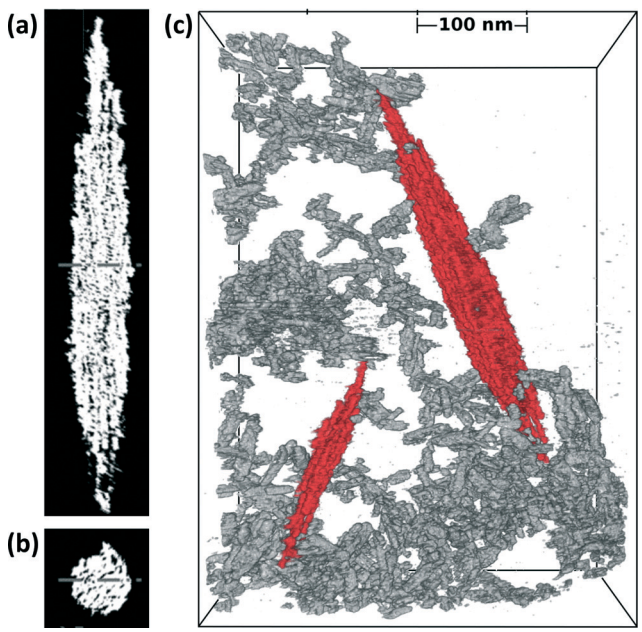

Fig. 5 Cryo-TEM tomographs. (a)–(b) Cross sections of the large hematite spindle in (c). (c) Broad-field view of akaganeite particles (grey) in 3D-network with hematite spindles (red).

particle aggregation state *in aqua* in three dimensions. Fig. 5c shows a broad field-of-view 3D cryo-TEM image of a vitrified sample after aging for 56 h, where akaganeite particles are aggregated into extensive open networks around hematite. Five or more groups of akaganeite particles (grey colored) are in close proximity of each of the two hematite spindles (red colored) in Fig. 5c. Examples of close-proximities have been verified from tilted views. 2D-cryo-TEM images in Fig. 2d–e also indicate akaganeite crystals in close contact with the hematite spindles. Typically, hematite spindles are found in close contact with akaganeite particles, but the number of particle contacts per spindle varies a lot (say between 0 and 20).

Dissolved iron concentrations were compared with chemical equilibrium calculations using MINTEQ. These calculations show that our starting solutions (20 mM $FeCl_3$, 0.45 mM NaH_2PO_4, pH 2.2) should reach equilibrium with bulk hematite ($\log[\{Fe^{3+}\}^2/\{H^+\}^6] = -1.418$) at a pH of 1.3 and a dissolved iron concentration of 0.28 mM. The pH values are in good agreement with measurements, and dissolved iron concentrations (~1 mM at 102 hours) are moderately higher than expected.

From the X-ray diffraction data, which provide relative weight fractions of akaganeite and hematite, and from the TEM data, which provide detailed information on particle shape and size distributions, we estimated the particle concentrations in samples recovered at each time-point. From this, we calculated that the number of akaganeite particles decreased by two orders of magnitude, from 1×10^{21} m^{-3} at 23 h to 2×10^{19} m^{-3} at 102 h. The number of hematite particles is roughly constant over time (~1×10^{17} m^{-3}). Even at 102 h, when the suspension is dominated by hematite spindles on a mass basis, akaganeite nanoparticles still outnumber hematite particles, but the reactive surface areas of akaganeite and hematite are comparable.

Discussion of the growth model

Our TEM observations show clear evidence for growth of akaganeite particles by oriented aggregation, where the particles (Fig. 6i) aggregate, align, and subsequently fuse to form a single crystal (Fig. 6ii). Many larger akaganeite particles have irregular surface morphology and appear to consist of two or three rods sitting directly side by side (Fig. 2b). In some cases, particles were aligned, but have not yet fused (Fig. 2a, c). Such aggregate-like particle morphologies with single-crystalline, low-angle or twin boundaries are often found in nanoparticle systems that grow by oriented aggregation.[22,23] Our evidence is comparable to that reported previously to indicate the operation of this growth mechanism, a pathway that was recently directly confirmed for a similar iron oxyhydroxide phase by *in situ* high-resolution TEM experiments.[6]

We suggest that the formation of the early-stage hematite spindles is driven by aggregation of akaganeite rods (Fig. 6iii), *i.e.*, akaganeite rods aggregate until the resulting particles reach a size where transformation to hematite is favorable. Size-driven phase transformations are common in the iron (oxyhydr)oxide systems.[24] In all cases (Fig. 4), hematite spindles were larger than 15 nm by 150 nm, which is significantly larger than the vast majority of akaganeite rods. Hematite has a larger interfacial energy than akaganeite, and therefore the transformation from akaganeite to hematite by dehydration and atomic rearrangement is thermodynamically favored only for large particles (surface area <2000 m^2 mol^{-1} and particle width greater than 4 nm).[24] However, we still observe relatively large akaganeite particles, >4 nm, that have not been converted to hematite. Such particles would be metastable, and a large energy barrier clearly exists with respect to their dehydration and recrystallization. Regarding the initial formation of hematite, we speculate that akaganeite–akaganeite interfaces may serve as favorable sites for the nucleation of hematite. Phase transformation driven by oriented attachment has been proposed previously. For example, the twin interface that can form during oriented attachment-based growth of anatase (TiO_2) shares some structural characteristics with rutile, and thus may serve to nucleate thermally-driven transformation to rutile.[25] Due to the relatively low number of hematite spindles, we infer that the correct attachment is a somewhat rare event (*i.e.*, it is not due to the commonly observed fusions of (100) and (001) planes of akaganeite). Although the precise interface that would favor transformation is unknown, less prominent surface features such as (010) steps and ledges may play a role; configurations that generate face-sharing octahedra would seem to favor hematite formation. The rate of spindle formation is evidently higher during the first hours of hydrolysis, as we observe that the number remains constant during the later stages of the experiment (from 23 to 102 h). The reduced formation rate of spindles later during the experiment may be due to changing thermodynamic conditions (as pH and supersaturation drop), or due to changes in surface morphology of the primary akaganeite particles.

The nano-porous structure of hematite spindles suggests construction from crystallographically aligned (and nearly aligned) subparticles, as found for growth by oriented attachment.[4,18,26,27] It was proposed that similarly synthesized hematite spindles have formed by aggregation of hematite nanoparticles.[9–11] This idea has been very strongly argued against, in favor of a process where akaganeite dissolves and reprecipitates as hematite.[8,12] Sugimoto and Muramatsu[12] make a strong case that the formation of hematite spindles

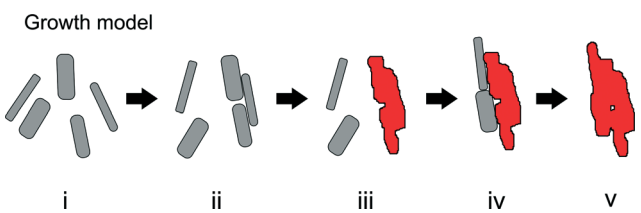

Fig. 6 Growth model. Akaganeite particles (grey rectangles, i) aggregate (ii) and transform to hematite spindles (red structures, iii). After the "incubation period" (i–iii), the hematite spindles grow more rapidly through aggregation of akaganeite particles (iv) followed by phase transformation of akaganeite to hematite (v).

cannot be due to the continuous precipitation and aggregation of individual hematite nanoparticles, based on their observations that the final number of spindles can be manipulated by adding hematite seeds (<5 nm diameter) to the solution. If small hematite particles were continuously generated in the solution, such seed particles would not have a major impact on the final product. Notably, we observe no sign of small hematite nanoparticles in the solution. Also, as our chemical analyses show a low Fe concentration and low pH after the initial (<1 h) nucleation burst of akaganeite particles, it is unlikely that hematite particles could be continuously nucleated homogenously within the next 160 h of heat treatment. We therefore agree with Sugimoto and Muramatsu[12] but note that their analysis does not preclude the possibility that the aggregation involves akaganeite onto hematite, followed by phase transformation.

A recent paper[11] studied cryo-plunged $FeCl_3$(aq)-samples that had aged in an autoclave at 160–200 °C and found that individual hematite nanoparticles exist as the sole precursors to hematite spindle formation. At this temperature, dehydration of individual precursor particles would be more strongly favored than in our experiments, and growth by hematite nanoparticle aggregation may be favored.

Only the precursor nano-scale akaganeite and the end product hematite spindles are detectable in our samples. The constant number of hematite spindles throughout the experiment (from 23 h to 102 h) indicates that hematite spindle nucleation is completed during the first hours of hydrolysis and the primary process controlling hematite formation thereafter is growth (not nucleation). This conclusion is supported by the high monodispersity of the spindle size distribution at all time-points (Fig. 4c).

The *in aqua* cryo-TEM finding of akaganeite and hematite particles in extended aggregate networks requires an altered view of particle interactions in suspension. Traditional models of stable colloidal suspensions, based on DLVO theory, posit that electrostatic repulsion inhibits direct contact between particles and the formation of large clusters.[28] However, in this suspension, we show extensive direct contact between particles, *i.e.*, a large fraction of the particles participate in a network, which may provide opportunities for enhanced crystal growth.

The simplest explanation for the observed hydrothermal growth of monodisperse micron-sized nanoporous hematite spindles at 100 °C is that akaganeite particles transform to hematite upon making suitable contact with a hematite surface (Fig. 6iv, v). Such a process is also consistent with prior studies that have shown that aggregation of nanoparticles can alter nanoparticle crystallinity[29] and that surface-bound molecules may induce phase transformations in nanoparticles.[30] Thus, we suggest that akaganeite–hematite interfaces promote dehydration and atomic rearrangement of newly attached akaganeite particles into the larger and thermodynamically more stable hematite. We did not observe intergrowths of akaganeite within hematite, suggesting that the reaction occurs rapidly upon suitable attachment.

The coarsening of the hematite spindles that occurs simultaneously with growth *via* aggregation is most likely caused by ion addition of dissolved iron. This seems reasonable since the iron concentration is quite high, probably due the solubility of akaganeite at low pH and the presence of small akaganeite particles (≤5 nm in diameter) like those circled in Fig. 2c.

In summary, we propose the growth, aggregation and transformation model shown in Fig. 6, where growth and phase transition are induced first by oriented aggregation of primary particles and later by aggregation of primary particles onto secondary particles. We speculate that this model may be applicable in explaining growth and phase transitions in other two-phase systems where particle aggregation exists and where ion concentrations and pH do not permit homogenous nucleation of the secondary particles. Detailed investigations of the interfaces and nanoparticle arrangements that may facilitate phase transitions are of much interest for further exploration.

Acknowledgements

CF acknowledges funding from the Danish Councils for Independent Research. HZ and JFB acknowledge financial support from the U.S. National Science Foundation (grant no. CHE-1213835). LRC, HZ, JFB and BL also acknowledge support from the U.S. Department of Energy (grant no. DE-AC02-05CH11231). The authors acknowledge allocation of beam time at the Advanced Light Source, Lawrence Berkeley National Laboratory. The authors acknowledge support of the National Center for Electron Microscopy, Lawrence Berkeley Lab, which is supported by the U.S. Department of Energy under Contract # DE-AC02-05CH11231.

References

1 S. Kumar, Z. Wang, R. L. Penn and M. Tsapatsis, A Structural Resolution Cryo-TEM Study of the Early Stages of MFI Growth, *J. Am. Chem. Soc.*, 2008, **130**, 17284.
2 V. M. Yuwono, N. D. Burrows, J. A. Soltis and R. L. Penn, Oriented Aggregation: Formation and Transformation of Mesocrystal Intermediates Revealed, *J. Am. Chem. Soc.*, 2010, **132**, 2163.
3 J. Baumgartner, A. Dey, P. H. H. Bomans, C. L. Coadou, P. Fratzl, N. A. J. M. Sommerdijk and D. Faivre, Nucleation and Growth of Magnetite from Solution, *Nat. Mater.*, 2013, **12**, 310.
4 J. F. Banfield, S. A. Welch, H. Zhang, T. T. Ebert and R. L. Penn, Aggregation-Based Crystal Growth and Microstructure Development in Natural Iron Oxyhydroxide Biomineralization Products, *Science*, 2000, **289**, 751.
5 V. M. Yuwono, N. D. Burrows, J. A. Soltis, T. A. Do and R. L. Penn, Aggregation of Ferrihydrite Nanoparticles in Aqueous Systems, *Faraday Discuss.*, 2012, **159**, 235.
6 D. Li, M. H. Nielsen, J. R. Lee, C. Frandsen, J. F. Banfield and J. J. De Yoreo, Direction-Specific Interactions Control

Crystal Growth by Oriented Attachment, *Science*, 2012, **336**, 1014.

7 M. Ozaki, S. Kratohvil and E. Matijevic, Formation of Monodisperse Spindle-Type Hematite Particles, *J. Colloid Interface Sci.*, 1984, **102**, 146.

8 T. Sugimoto, A. Muramatsu, K. Sakata and D. Shindo, Characterization of Hematite Particles of Different Shapes, *J. Colloid Interface Sci.*, 1993, **158**, 420.

9 M. P. Morales, T. González-Carreño and C. J. Serna, The Formation of Alpha-Fe2O3 Monodispersed Particles in Solution, *J. Mater. Res.*, 1992, **7**, 2538.

10 M. Ocaña, M. P. Morales and C. J. Serna, The Growth-Mechanism of Alpha-Fe2O3 Ellipsoidal Particles in Solution, *J. Colloid Interface Sci.*, 1995, **171**, 85.

11 T. P. Almeida, M. V. Fay, Y. Q. Zhu and P. D. A. Brown, A Valve-Assisted Snapshot Approach to Understand the Hydrothermal Synthesis of Alpha-Fe2O3 Nanorods, *CrystEngComm*, 2010, **12**, 1700.

12 T. Sugimoto and A. J. Muramatsu, Formation Mechanism of Monodispersed Alpha-Fe2O3 Particles in Dilute FeCl3 Solutions, *J. Colloid Interface Sci.*, 1996, **184**, 626.

13 T. Sugimoto, Y. Wang, H. Itoh and A. Muramatsu, Systematic Control of Size, Shape and Internal Structure of Monodisperse Alpha-Fe2O3 Particles, *Colloids Surf., A*, 1998, **134**, 265.

14 J. R. Kremer, D. N. Mastronarde and J. R. McIntosh, Computer Visualization of Three-Dimensional Image Data Using IMOD, *J. Struct. Biol.*, 1996, **116**, 71.

15 J. I. Agulleiro and J. J. Fernandez, Fast Tomographic Reconstruction on Multicore Computers, *Bioinformatics*, 2011, **27**, 582.

16 V. Kaynig, T. Fuchs and J. M. Buhmann, Neuron Geometry Extraction by Perceptual Grouping in ssTEM Images, *Computer Vision and Pattern Recognition*, IEEE Conference, San Francisco, CA, June 13–18, 2010.

17 J. Q. Jiang and N. J. D. Graham, Observations of the Comparative Hydrolysis/Precipitation Behaviour of Polyferric Sulphate and Ferric Sulphate, *Water Res.*, 1998, **32**, 930.

18 L. Lutterotti, Total Pattern Fitting for the Combined Size-Strain-Stress-Texture Determination in Thin Film Diffraction, *Nucl. Instrum. Methods Phys. Res., Sect. B*, 2010, **268**, 334.

19 J. E. Post, P. J. Heaney, R. B. Von Dreele and J. C. Hanson, Neutron and Temperature-resolved Synchrotron X-ray Powder Diffraction Study of Akaganeite, *Am. Mineral.*, 2003, **88**, 782.

20 R. L. Blake and R. E. Hessevick, Refinement of the Hematite Structure, *Am. Mineral.*, 1966, **51**, 123.

21 J. W. Christian, *The Theory of Transformations in Metals and Alloys*, Elsevier, Amsterdam, Netherlands, 3rd edn, 2002, p. 546.

22 R. L. Penn and J. F. Banfield, Imperfect Oriented Attachment: Dislocation Generation in Defect-Free Nanocrystals, *Science*, 1998, **281**, 969.

23 R. L. Penn, J. J. Erbs and D. M. Gulliver, Controlled Growth of Alpha-FeOOH Nanorods by Exploiting-Oriented Aggregation, *J. Cryst. Growth*, 2006, **293**, 1.

24 A. Navrotsky, L. Mazeina and J. Majzlan, Size-Driven Structural and Thermodynamic Complexity in Iron Oxides, *Science*, 2008, **319**, 1635.

25 R. L. Penn and J. F. Banfield, Formation of Rutile Nuclei at Anatase {112} Twin Interfaces and the Phase Transformation Mechanism in Nanocrystalline Titania, *Am. Mineral.*, 1999, **84**, 871.

26 R. L. Penn and J. F. Banfield, Morphology Development and Crystal Growth in Nanocrystalline Aggregates under Hydrothermal Conditions: Insights from Titania, *Geochim. Cosmochim. Acta*, 1999, **63**, 1549.

27 M. Niederberger and H. Coelfen, Oriented attachment and mesocrystals: Non-Classical Crystallization Mechanisms Based on Nanoparticle Assembly, *Phys. Chem. Chem. Phys.*, 2006, **8**, 3271.

28 J. Addai-Mensah and C. A. Prestidge, Structure Formation in Dispersed Systems, in *Coagulation and Flocculation*, ed. H. Stechemesser and B. Dobias, CRC Press, 2005.

29 F. Huang, B. Gilbert, H. Zhang and J. F. Banfield, Reversible, Surface-Controlled Structure Transformation in Nanoparticles Induced by an Aggregation State, *Phys. Rev. Lett.*, 2004, **92**, 155501.

30 C. M. Goodell, B. Gilbert, S. J. Weigand and J. F. Banfield, Kinetics of Water Induced Structural Transformation in ZnS nanoparticles, *J. Phys. Chem. C*, 2008, **112**, 4791.

